Developmental Cognitive Neuroscience 12 (2015) 74–85

Contents lists available at ScienceDirect

Developmental Cognitive Neuroscience

journal homepage: http://www.elsevier.com/locate/dcn

In vivo evidence of neurophysiological maturation of the human adolescent striatum

Bart Larsen [a,b,*], Beatriz Luna [a,b,c]

[a] Department of Psychology, University of Pittsburgh, Pittsburgh, PA 15213, USA
[b] Center for the Neural Basis of Cognition, Pittsburgh, PA 15213, USA
[c] Western Psychiatric Institute and Clinic, University of Pittsburgh Medical Center, Pittsburgh, PA 15213, USA

ARTICLE INFO

Article history:
Received 29 July 2014
Received in revised form
17 December 2014
Accepted 18 December 2014
Available online 30 December 2014

Keywords:
Adolescence
Striatum
Development
Neurophysiology
T2*
Multivariate pattern analysis

ABSTRACT

Maturation of the striatum has been posited to play a primary role in observed increases in adolescent sensation-seeking. However, evidence of neurophysiological maturation in the human adolescent striatum is limited. We applied T2*-weighted imaging, reflecting indices of tissue–iron concentration, to provide direct in vivo evidence of neurophysiological development of the human adolescent striatum. Multivariate pattern analysis (MVPA) of striatal T2*-weighted signal generated age predictions that accounted for over 60% of the sample variance in 10–25 year olds, using both task-related and resting state fMRI. Dorsal and ventral striatum showed age related increases and decreases respectively of striatal neurophysiology suggesting qualitative differences in the maturation of limbic and executive striatal systems. In particular, the ventral striatum was found to show the greatest developmental differences and contribute most heavily to the multivariate age predictor. The relationship of the T2*-weighted signal to the striatal dopamine system is discussed. Together, results provide evidence for protracted maturation of the striatum through adolescence.

1. Introduction

Adolescent behavior is characterized by increases in sensation-seeking that can lead to maladaptive risk-taking, resulting in increased likelihood of death or serious injury (Eaton et al., 2006). Thus, there is an impetus to understand the neurodevelopmental changes in the motivational system that may contribute to this behavioral profile. The striatum is of particular interest in this context because of its involvement in motivation and reward processing as well as learning, motor control, and cognition (Haber and Knutson, 2010; McClure et al., 2003; Middleton and Strick, 2000; Vo et al., 2011).

Rodent and non-human primate models provide evidence indicating continued striatal synaptogenesis in early adolescence, peaks in dopamine receptor expression and dopamine projections from the striatum to prefrontal cortex, and synaptic pruning in late adolescence (Crews et al., 2007; Kalsbeek et al., 1988; Rosenberg and Lewis, 1995; Tarazi et al., 1998; Teicher et al., 1995). This line of evidence has led to the hypothesis that similar neurophysiological changes are occurring in adolescent humans (Casey et al., 2008; Spear, 2000). Initial functional magnetic resonance imaging (fMRI) studies have found compelling evidence suggesting peak sensitivity of the adolescent striatum to reward stimuli relative to adults and children (Ernst et al., 2005; Galvan et al., 2006, 2007; Geier et al., 2010; Leijenhorst et al., 2010; Padmanabhan et al., 2011), though

* Corresponding author at: 121 Meyran Avenue, Room 109, Pittsburgh, PA 15231, USA. Tel.: +1 412 383 5233.
E-mail addresses: bslarsen1@gmail.com, bsl18@pitt.edu (B. Larsen).

http://dx.doi.org/10.1016/j.dcn.2014.12.003

this finding has not been consistent (Bjork et al., 2004; Eshel et al., 2007) and likely depends on the reward context investigated (Crone and Dahl, 2012). For example, recent work has suggested that striatal reactivity to reward anticipation increases into adulthood while reactivity to reward receipt decreases (Hoogendam et al., 2013). Currently there is a lack of in vivo measures with which to assess age-related differences in human striatal neurophysiology which limits our ability to understand neural mechanisms underlying differences in adolescent striatal function. Understanding the development of striatal neurophysiology is of particular significance given that abnormal striatal neurophysiology and function are implicated in a range of neuropsychological disorders that emerge during childhood and adolescence (Bradshaw and Sheppard, 2000; Chambers et al., 2003). An improved understanding of normative neurophysiological maturation of the striatum can thus inform models of normal and abnormal adolescent behavior.

Tissue–iron concentration is predominant in the striatum (Haacke et al., 2005; Schenck, 2003) and has been found to support dopamine D2 receptor and dopamine transporter (DAT) densities in studies of iron deficiency, ADHD, and restless leg syndrome, which are related to abnormalities in DA processing, (Adisetiyo et al., 2014; Connor et al., 2009; Erikson et al., 2000; Wiesinger et al., 2007), as well as the function and regulation of dopamine neurons (Beard, 2003; Jellen et al., 2013). As such, differences in striatal tissue iron concentration, which can be measured using MRI, can potentially serve as an indicator of dopaminergic differences in adolescence. Tissue–iron is paramagnetic and thus strongly influences the T2*-weighted MRI signal (Langkammer et al., 2010, 2012; Schenck, 2003), which can be non-invasively collected in vivo throughout the lifespan (Aquino et al., 2009; Haacke et al., 2005; Wang et al., 2012). The influence of iron on the T2* signal has been used to quantify iron in a variety of MR measures, including susceptibility weighted imaging (SWI) (Haacke et al., 2004), R2* (Haacke et al., 2010), and R2′ (Sedlacik et al., 2014). In this study, we make use of a large T2*-weighted echo-planar imaging (EPI) dataset, most akin to SWI. Initial studies have used similar data in conjunction with multivariate pattern analysis to investigate the striatal processes underlying learning (Vo et al., 2011).

Here we use T2*-weighted EPI (T2*) to characterize age-related differences in the neurophysiology of the human adolescent striatum in vivo using a multivariate pattern analysis approach. Specifically we use spatial patterns of striatal T2* to generate highly significant age predictions from both task-related and resting state T2*-weighted EPI (fMRI) acquisitions, demonstrating the strong and robust relationship between this measure and development. Furthermore, we identify the ventral striatum, a central hub of dopamine reward pathways hypothesized to underlie adolescent risk-taking (Blum et al., 2000; Casey et al., 2008; Spear, 2000), as a critical component of adolescent striatal maturation. This work highlights the dynamic nature of normative adolescent striatal development, informing models of the maturation of motivational systems during adolescence.

2. Materials and methods

2.1. Sample

One hundred and sixty adolescents and young adults participated in this study (ages 10–25, $M = 16.56$, $SD = 3.62$). Eighteen participants were excluded due to excess head movement (described below), yielding a final sample of 142 (ages 10–25, $M = 16.41$, $SD = 3.71$, 71 male). A subset of these were also included in a replication analysis using resting-state data (described below). All subjects had medical histories that revealed no neurological disease, brain injury, and no history of personal or first-degree relative with major psychiatric illness. All experimental procedures in this study complied with the Code of Ethics of the World Medical Association (1964 Declaration of Helsinki) and the Institutional Review Board at the University of Pittsburgh. Participants were paid for their participation in the study. These data were initially collected for a project investigating reward processing and resting state functional connectivity and subsets of this dataset were included in previously published studies of resting state network development (Hwang et al., 2013) and incentive processing (Paulsen et al., 2014).

2.2. Imaging procedure

Imaging data were collected using a 3.0 Tesla Trio (Siemens) scanner at the Magnetic Resonance Research Center (MRRC), Presbyterian University Hospital, Pittsburgh, PA. The acquisition parameters were: TR = 1.5 s; TE = 25 ms; flip angle = 70°; single shot; full *k*-space; 64×64 acquisition matrix with FOV = 20 cm × 20 cm. Twenty-nine 4 mm-thick axial slices with no gap were collected, aligned to the anterior and posterior commissure (AC–PC line), generating 3.125 mm × 3.125 mm × 4 mm voxels, which covered the entire cortex and most of the cerebellum. We collected four runs of 302 TRs during the antisaccade task ($4 \times 302 = 1208$) and one run of 200 TRs during the resting-state scan. A three-dimensional volume magnetization prepared rapid acquisition gradient echo (MPRAGE) pulse sequence with 192 slices (1 mm slice thickness) was used to acquire the structural images in the sagittal plane.

T2*-weighted data were collected as part of a separate study investigating reward processing. Briefly, subjects participated in a reward modulated antisaccade task, in which they were instructed to make saccades to the mirror locations of peripherally presented stimuli. At the start of each trial, subjects were presented with either a reward, loss, or neutral cue that indicated the possibility of reward dependent on performance. Performance was evaluated using eye-tracking and participants received auditory feedback for correct and incorrect trials.

2.3. Resting-state dataset

One hundred subjects also participated in a resting state scan. Eleven were excluded due to motion artifacts and thus 89 subjects were included in this analysis (ages 10–25, $M = 16.2$, $SD = 3.77$; 43 male). We collected a 5 min

(200 volumes) resting-state scan for each subject using the same scan parameters listed above. During the resting-state scan, participants were asked to close their eyes, relax, but not fall asleep.

2.4. Preprocessing of T2*-weighted data

All preprocessing was done using FMRIB Software Library (FSL; Smith et al., 2004) and the Analysis of Functional Neuro Images (AFNI) software package (Cox, 1996). Initial preprocessing steps are similar to those used in conventional fMRI. T2*-weighted data was initially despiked and slice time corrected to account for sequential acquisition. To address motion, we used rotational and translational head motion estimates to calculate root mean square (RMS) movement measures, and participants with relative RMS greater than a stringent threshold of 0.3 mm for more than 15% of volumes in a run were excluded from further analysis. For the remaining subjects, we applied motion correction by aligning each volume in the time series to the volume obtained in the middle of the acquisition. Each participant's T2*-weighted data was linearly registered to the MPRAGE using FSL's FLIRT utility and then the MPRAGE image was nonlinearly registered into MNI (Montreal Neurological Institute) space using FSL's FNIRT utility. The concatenation of the linear registration from EPI to MPRAGE and the nonlinear registration from MPRAGE into MNI space was then applied to all EPI images for each participant. Volumes were high-pass filtered at .008 Hz. Data were not smoothed so as not to perturb voxel-wise patterns for the subsequent MVPA analysis. Smoothing can potentially bias the performance of linear support vector machines (Misaki et al., 2013). Resting-state and task-related data were processed separately using identical procedures.

2.4.1. Normalization and averaging

Commonly, T2*-weighted EPI data are analyzed across time, quantifying small fluctuations in the T2*-weighted signal related to the blood–oxygen-level dependent (BOLD) response. We wish to emphasize that in this study, we are not interested in these small BOLD fluctuations. Rather, we are interested in the properties of the T2*-weighted signal which do not change with time and are reflective of persistent neurophysiological properties of brain tissue. Thus, the preprocessing stream diverges from that of conventional BOLD analysis at this point. Procedures for processing our T2*-weighted images closely followed Vo et al. (2011). Each volume was first normalized to its own mean, and the normalized signal was then averaged, voxel-wise, across all four runs (1208 volumes) of the task acquisition. This process resulted in one normalized T2*-weighted image for each participant. Resting-state data were analyzed separately and were averaged across all 200 volumes from the 5 min acquisition. The normalization step is necessary because the T2*-weighted signal alone is sensitive to potential differences between MRI scans – either within subjects across time or between subjects – that can lead to shifts in T2*-weighted signal intensity. Normalization thus allows for comparison of T2* values across participants. Though T2* signal could be calculated from a single volume, we averaged across volumes to enhance the signal to noise ratio.

2.5. Identification of striatal regions

We anatomically identified the putamen, caudate, and nucleus accumbens according to brain atlases included in the AFNI software package. Region masks were made more conservative by removing any voxels likely to contain cerebrospinal fluid (CSF). CSF was parcellated using FSL's FAST segmentation, and voxels that had an average subject-wise probability greater than 0.15 of being CSF were removed from anatomically defined regions.

2.6. Univariate analysis

We first applied a traditional univariate analysis to assess mean level developmental differences in striatal T2*. For each subject, we computed the spatial mean T2*-weighted signal intensity across voxels within an anatomically defined region and analyzed the relationship between spatial means and chronological age. Specifically, we regressed age on mean T2* values using simple regression and computed the Pearson correlation between the fitted values of age and the true ages of subjects within each region of interest.

2.7. Multivariate pattern analysis

It is well established that the striatum and its subregions (caudate, putamen) are not spatially homologous in function, connectivity, or neurobiology (Cohen et al., 2009; Martinez et al., 2003; Middleton and Strick, 2000; Postuma and Dagher, 2006). Further, the structural development of the striatum progresses in a spatially non-uniform fashion (Raznahan et al., 2014). Therefore, the development of underlying striatal neurophysiology, including tissue–iron concentration, is likely also non-uniform. Thus, we hypothesized that age-related differences in striatal T2* would be better captured by a more sensitive, multivariate approach. To analyze the relationship between fine-grained patterns of T2* intensity and age, we applied multivariate linear support vector machine regression (SVR) in MATLAB (The MathWorks, Inc., Natick, Massachusetts, USA) using LIBSVM (Chang and Lin, 2011). Support vector regression has become a popular analysis tool in neuroimaging studies due to its ability to handle high-dimensional datasets and generate accurate predictions (Misaki et al., 2010). The multivariate approach allows for the assessment of changes in voxel-wise patterns of T2* in the striatum that relate to age. Importantly, this analysis has advantages over conventional averaged region of interest univariate analyses in that it is sensitive to potential spatial heterogeneity of developmental T2* trajectories across the striatum that are not captured by a mass spatial average. Of particular relevance to this study, SVR was previously used by Vo et al. (2011) to predict learning success from spatial patterns of striatal T2*, and by Dosenbach et al. (2010) to predict age from patterns of resting-state functional connectivity. Support vector machines have been described in detail from both a practical (Luts et al., 2010; Pereira et al., 2009) and

detailed mathematical point of view (Burges Christopher, 1998; Chih-Wei et al., 2003; Vapnik, 1999), and will only be described briefly here.

Linear support vector regression is an extension of support vector classification that allows for the association of feature patterns with a real-valued variable, thus allowing for real-valued predictions. Samples (data points) with real-valued labels are represented in a high-dimensional space with dimensions equal to the amount of features of a variable of interest. SVR defines a regression line through the high-dimensional feature space that optimally models the functional relationship between the features of a variable, x (e.g. voxel-wise T2* values in a region of interest), and the real-valued labels of a variable, y (e.g. the age of a subject). Samples are penalized in proportion to their distance from the regression line. We applied epsilon insensitive SVR which defines a tube around the regression line with width controlled by the parameter, epsilon, inside of which samples incur no penalty. The trade-off between the degree to which samples that fall outside the epsilon insensitive tube are penalized and the flatness of the regression line is controlled by the constant, C. As the value of C increases, the regression line is allowed to be less flat, which can increase the generalizability of the model.

We trained and validated our SVR model across subjects (one set of voxel-wise T2* values and one age label per subject) using leave-one-subject-out (LOSO) cross-validation. LOSO is an iterative process in which one subject's data is used for validation while the other $n-1$ subjects are used for training. An age prediction is generated for the left out sample based on voxel-wise T2* values alone, and the process is repeated until every subject has been used for validation. This results in one age prediction for each subject, and the performance of the SVR model can be determined by the correlation between true subject ages and those predicted by the model. The parameter C was optimized for each fold of LOSO cross-validation using nested LOSO cross-validation. We used the default value of epsilon from the LIBSVM toolbox of 0.001. The SVR analysis was repeated for resting-state T2* data. All p-values were confirmed via random permutation significance tests (1000 iterations). We chose LOSO rather than other methods of cross-validation in order to maximize the amount of training data used in each cross-validation iteration; though our sample size is large, the number of subjects in the sample was often less than the number of features included in the SVR model.

2.7.1. Partial volume correction

To ensure that multivariate age predictions were not simply reflecting potential systematic differences in T2* arising from partial volume effects, we used FSL's FAST tissue segmentation tool to create probability masks of white and gray matter from participants' T1-weighted images. We then regressed gray matter probabilities out of the T2* measure across subjects for each voxel and repeated the SVR analysis using the corrected data. In addition to controlling for systematic differences in partial voluming, this process orthogonalized age-related differences in T2* values with respect to potential differences in striatal volume and nonlinear spatial normalization.

2.7.2. Pattern characterization

To characterize the spatial patterns of striatal T2* and their trajectory with age, we estimated the developmental trajectory of T2* by regressing age on T2* signal using linear, quadratic, and inverse regression models for each striatal voxel used in the SVR analysis. To quantify the relative contribution of components (voxels) of the spatial patterns of T2*, we computed the absolute value of the average feature weight for each striatal voxel used in the SVR analysis across all folds of LOSO cross-validation.

2.8. Searchlight analysis

To explore the relationship between T2* intensity and age beyond our a priori striatal regions, we performed a whole-brain searchlight analysis (Kriegeskorte et al., 2006). To conduct the analysis, we defined a spherical template with a diameter of 5 voxels (81 voxels total), centered the template on each brain voxel in turn, and performed the SVR analysis described above on the 81 voxels in the template. Only voxels included in a conjunction brain mask were included in this analysis. The correlation between true and predicted age at each template location was stored at the center voxel. By repeating this process for each voxel, we obtained a whole-brain mask of correlations. The locations of voxel clusters were estimated using atlases included in AFNI.

3. Results

3.1. Univariate analysis

The spatial mean of T2* across all voxels in the striatum was not significantly related to age ($r = 0.02$), with the model accounting for only 0.0004% of variance in the sample. When we segmented the striatum into the caudate, putamen, and nucleus accumbens and repeated the analysis, we found that the information carried in mean T2* was sufficient to generate significant age predictions in the caudate ($r = 0.286$, $p < 0.001$) and putamen ($r = 0.182$, $p < 0.05$), and was particularly predictive in the nucleus accumbens ($r = 0.506$, $p < 10^{-9}$, Fig. 1A, white bars). However, functional and neurobiological subdivisions of the striatum exist at a finer scale than can be captured by spatial mean level analysis (Cohen et al., 2009; Martinez et al., 2003; Postuma and Dagher, 2006). Therefore, we hypothesized that developmental differences in striatal T2* would be better captured using a more sensitive, multivariate approach.

3.2. Multivariate pattern analysis

Multivariate patterns of T2* signal produced highly significant age predictions in all striatal regions (Fig. 1A, black bars), indicating a strong relationship between this measure and adolescent development. The greatest correlation between predicted age and true participant age was observed in the whole striatum (combined caudate, putamen, and nucleus accumbens), where T2* patterns

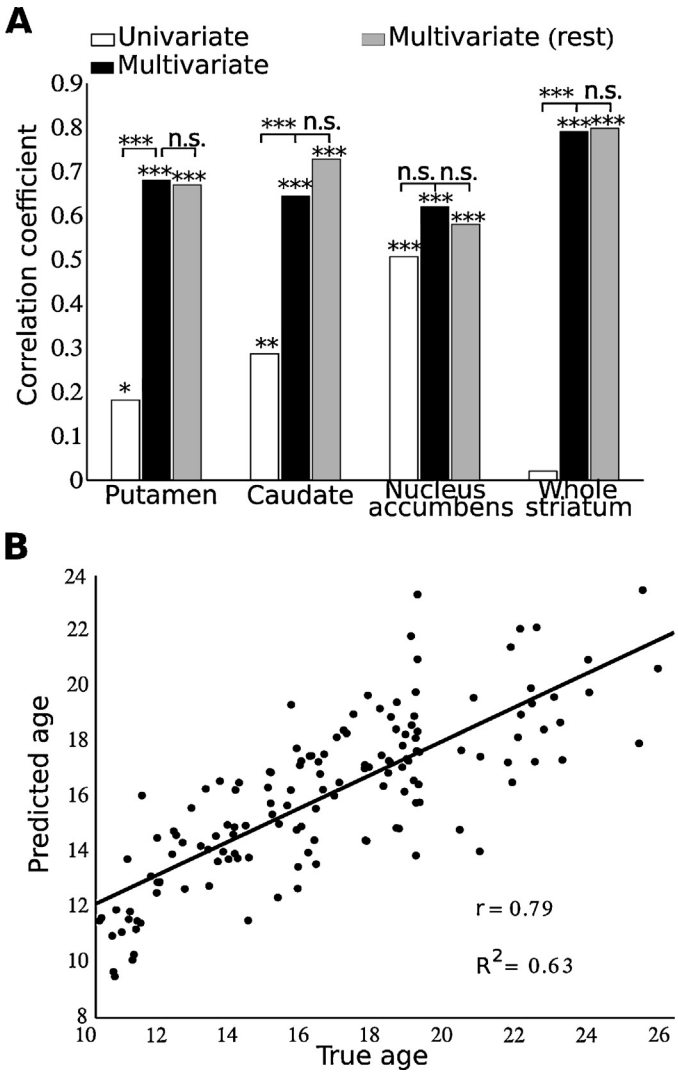

Fig. 1. Correlations between true age and predicted age using T2* from univariate and multivariate models in striatal ROIs. (A) Bar graphs comparing correlations between true and predicted age using three models: univariate analysis (white bars) and multivariate pattern analysis of both task (black bars) and rest (gray bars) data. Multivariate analysis yields significantly greater correlation than univariate analysis in the putamen, caudate, and whole striatum. There is no difference between task-related and resting-state results. ($^{*}p < 0.05$, $^{**}p < 0.01$, $^{***}p < 0.001$ permutation tests). (B) True vs. predicted age from the whole striatum using multivariate pattern analysis of T2* in 142 adolescents and young adults. Predicted age accounts for 63% of the sample variance.

accounted for 63% of variance in participant age ($r = 0.79$, $p < 10^{-30}$; permutation test: $p < 0.001$, Fig. 1B).

Striatal gray matter volume varies with age over adolescence (Raznahan et al., 2014; Sowell et al., 1999). To ensure that multivariate age predictions were not reflecting systematic partial volume differences arising from changing striatal volume or artifacts of spatial normalization, we repeated the SVR analysis controlling for voxel-wise differences in gray-matter volume. We found no significant difference in model performance using volume controlled data (supplementary Fig. 1).

The T2* signal reflects persistent neurophysiological tissue properties (Vo et al., 2011) and should be insensitive to task or context effects. Nevertheless, we replicated the analysis for subjects who had participated in a resting state study during the same scan session. We found no significant difference in our ability to predict age from patterns of T2* using task-related and resting state data (Fig. 1B, gray bars). Furthermore, we computed the voxel-wise correlation between spatial patterns of resting state and task-related T2* in the striatum for each participant and observed a median Pearson correlation of 0.97, indicating that patterns are consistent between task and rest. Thus, here forward we limit our focus to T2* data collected during task, which is averaged over more volumes (1208 vs 200) and has a greater sample size (142 vs 89).

As we predicted, spatial patterns predicted age more accurately for nearly every striatal region of interest. The improvement was particularly striking in whole striatum where the amount of explained variance in participant age increased from close to 0% using spatial means to 63% using spatial patterns. This contrast strongly indicates

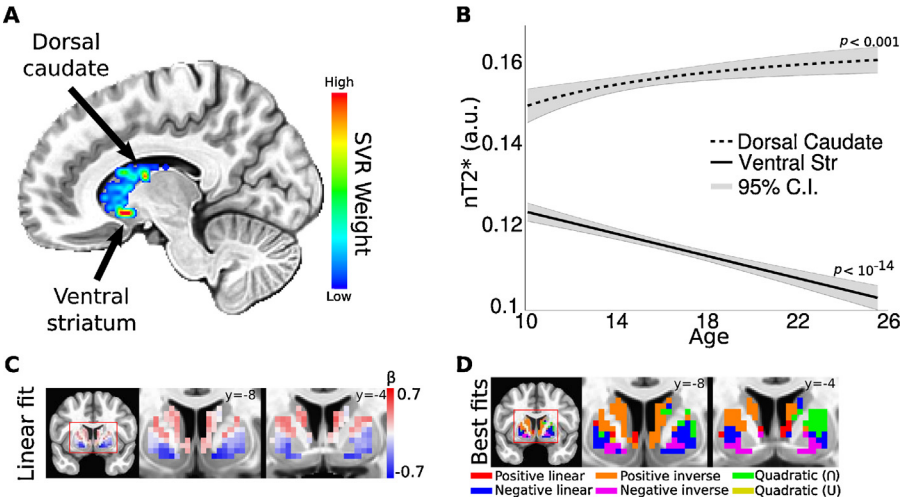

Fig. 2. Characterizing multivariate patterns of striatal maturation. (A) Quantification of absolute feature weights for all striatal voxels included in the multivariate SVR model. Higher weights indicate greater relative contributions to the multivariate predictor. The highest weighted voxels were clustered in the ventral striatum and dorsal caudate. (B) Average developmental T2* trajectories and 95% confidence intervals for voxels from peak clusters in (B) plotted as a function of age. Panels C and D illustrate the maturational trajectories of individual voxels included in the multivariate SVR analysis. (C) Standardized beta estimates from voxel-wise simple linear regressions of age on T2*. Maturational trajectories fell along a dorsal–ventral gradient, with voxel T2* values generally increasing with age dorsally, to generally decreasing ventrally. This relationship is symmetric across hemispheres. (D) Striatal voxels from (C) color-coded according to best fitting model (linear: red/blue, inverse: orange/magenta, quadratic: green/yellow).

that the striatum undergoes a complex pattern of neurophysiological development reflected throughout striatal voxels over adolescence. To better elucidate the nature this developmental pattern, we characterized developmental trajectories of T2* across the striatum.

3.3. Pattern characterization

A key advantage of SVR is the ability to quantify the features that contribute to the multivariate predictor. To make use of this quantitative information, we extracted the feature weights assigned to each voxel from the SVR analysis. A feature weight can be thought of as an index of the importance of a feature (voxel) in generating the multivariate age prediction. To determine the components of the spatial pattern of striatal T2* intensities that had the greatest relative contribution to the multivariate predictor, we quantified absolute feature weights to identify the striatal voxels with the greatest relative weight. A cluster of voxels in the ventral striatum, at the junction of the caudate, putamen, and nucleus accumbens were most influential, followed by a cluster in dorsal caudate (Fig. 2A). The ventral striatal cluster had a negative linear association with age ($R^2 = 0.361$, $p < 10^{-14}$; Fig. 2B solid line), and the dorsal caudate cluster had an increasing inverse association with age ($R^2 = 0.078$, $p < 0.001$; Fig. 2B dashed line).

Though these clusters had the greatest relative weighting, it is important to keep in mind that the age prediction is a function of the multivariate relationship amongst all voxels included in the model. Therefore, we estimated the developmental trajectory of T2* signal for each voxel used in the SVR analysis using simple linear, quadratic, and inverse regression models known to characterize developmental change during this period (Luna et al., 2004) in order to comprehensively visualize maturational patterns. The majority of voxels were linearly related with age, with a subset being best fit by quadratic and inverse relationships. To illustrate this distribution, we categorized voxels based on the best fitting model – positive and negative linear, quadratic, and inverse relationships – and overlaid them on a standard anatomical image, creating a developmental T2* mask of the striatum (Fig. 2D).

Descriptively, developmental T2* trajectories largely fell along a ventral to dorsal gradient, ranging from highly negative relationships in ventral portions of the striatum known to have predominantly limbic cortical connections to positive relationships in dorsal portions known to have predominantly executive and motor cortical connections (Alexander et al., 1986; Cohen et al., 2009), that was symmetric across hemispheres (Fig. 2C; recall increased tissue iron concentration *decreases* the T2* signal). Negative quadratic (inverted "U") and increasing inverse relationships were observed in dorsal portions of the putamen, caudate, and nucleus accumbens, with negative quadratic relationships (inverted "U" shaped) clustered more in the right hemisphere and increasing inverse relationships clustered more on the left. Negative quadratic relationships reached average maxima over adolescence at age 18.4 in the caudate and 17.4 in the putamen. Positive quadratic ("U" shaped) and decreasing inverse relationships were observed bilaterally in the ventral putamen, with decreasing inverse relationships occurring in rostroventral putamen and positive quadratic relationships occurring in the caudoventral putamen reaching minima at age 20. The observed heterogeneity in developmental trajectories across striatal voxels likely explains the greater performance of our multivariate model over the univariate model in capturing age-related differences.

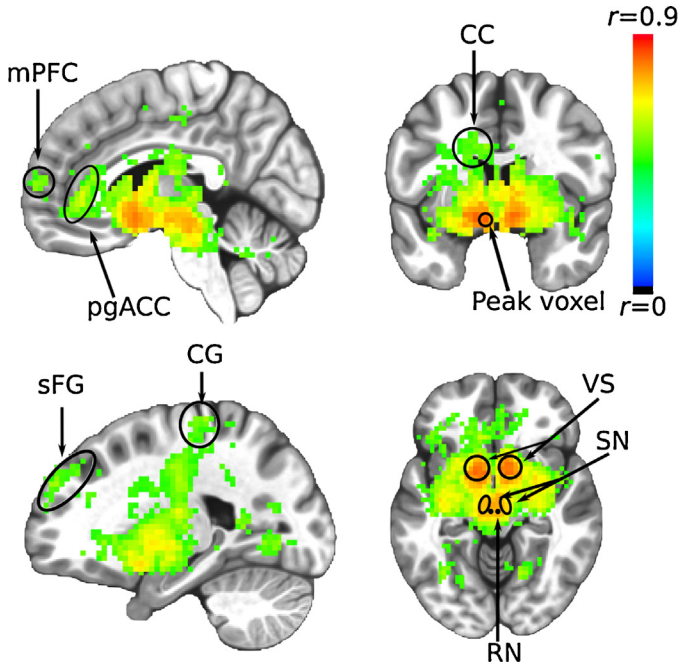

Fig. 3. Whole-brain searchlight results highlighting regions with strong associations between T2* and adolescent development. Colors represent the correlation between true age and predicted age from the SVR searchlight analysis centered at that voxel. Only voxels with correlations between true and predicted age that are significant at $p < 0.001$, Bonferroni corrected (i.e. 0.001/number of brain voxels) are displayed. The peak voxel is located in the ventral striatum (MNI coordinates: −8, 5, −11). mPFC: medial pre-frontal cortex, pgAC: perigenual anterior cingulate, CC: corpus callosum, sFG: superior frontal gyrus, CG: central gyrus, VS: ventral striatum (including nucleus accumbens), SN: substantia nigra, RN: red nucleus.

3.4. Whole-brain analysis

To investigate possible associations between spatial T2* patterns and development across the brain and to confirm the specificity of striatal contributions, we performed an exploratory searchlight analysis (Kriegeskorte et al., 2006). The searchlight revealed that age was predicted most significantly in the striatum and midbrain, including the red nucleus, substantia nigra, and other parts of the basal ganglia (Fig. 3). Other regions that generated highly significant age predictions include perigenual anterior cingulate cortex, Brodmann Area 10, medial pre-frontal cortex, anterior superior frontal gyrus, insula, pre- and post-central gyrus, anterior thalamus, and the dentate nucleus of the cerebellum. Significant correlations were also observed in the corpus callosum and fronto-parietal white matter structures. Many of these regions (e.g. basal ganglia, midbrain, dentate nucleus, frontal white matter) are among the most iron-rich areas of the brain (Connor and Menzies, 1996; Drayer et al., 1986; Haacke et al., 2005, 2007; Langkammer et al., 2010), and part of the mesolimbic/mesocortical and nigrostriatal dopamine pathways (e.g. midbrain, striatum, prefrontal cortex (Beaulieu and Gainetdinov, 2011; Haber and Knutson, 2010; Puglisi-Allegra and Ventura, 2012). The greatest correlations were observed at the juncture of the nucleus accumbens, ventromedial putamen, and ventromedial caudate (peak voxel: MNI −8, 5, −11), indicating that T2* has a particularly strong relationship with adolescent development in this part of the brain, which is strongly associated with dopaminergic reward pathways and the limbic system (Galvan et al., 2006, 2007; McGinty et al., 2013; Puglisi-Allegra and Ventura, 2012).

The T2*-weighted signal, particularly when collected in-plane as in EPI, is susceptible to signal dropout due to susceptibility artifacts near the base of the brain (e.g. orbitofrontal cortex and inferotemporal cortex), thus raising the possibility that age-related differences in T2* could arise from susceptibility artifacts in these brain areas. This should not have a large effect given that the gross morphometry of the brain is established by younger ages than our age group (Caviness et al., 1996). Moreover, (1) our most significant age effects occur in brain areas that are known to be high in iron concentration (e.g. basal ganglia and midbrain) and inset from areas with pronounced signal dropout and (2) that brain areas most prone to susceptibility artifacts (e.g. oribitofrontal cortex and inferotemporal cortex; supplementary Fig. 2A and B) do not show significant age effects (supplementary Fig. 2C).

4. Discussion

The present study used spatial patterns of striatal task-related and resting-state normalized T2*-weighted images to generate highly significant age predictions in a large cross-sectional sample of adolescents and young adults, providing in vivo evidence of neurophysiological development of the human striatum over adolescence. Spatial patterns of T2* were predictive of adolescent age in the striatum as a whole as well as in striatal subregions, caudate, putamen, and nucleus accumbens from as

little as five minutes of resting-state fMRI, demonstrating a strong association between T2* and adolescent development throughout the striatum.

4.1. The T2* signal

Critical for a full interpretation of these findings is an understanding of the neurophysiological components that contribute to the T2* signal. T2* is most strongly related to transverse (spin–spin) relaxation time, magnetic susceptibility of tissue, and magnetic field homogeneity. Thus, tissue–iron (non-heme) concentration and myelin concentration are the tissue types that contribute most strongly to the T2* signal (Aquino et al., 2009; Daugherty and Raz, 2013; Langkammer et al., 2012; Schenck, 2003). Both tissue–iron and myelin have long transverse relaxation times, thus causing a hypo-intense T2* signal (Aoki et al., 1989; Chavhan et al., 2009; He and Yablonskiy, 2009). However, myelin is diamagnetic and tissue–iron is paramagnetic, so tissue–iron has a greater contribution to T2* (greater hypo-intensity) as a consequence of its magnetic susceptibility and effect on magnetic field inhomogeneity (Langkammer et al., 2010; Schenck, 2003). Therefore, though tissue–iron and myelin both contribute to T2*, the signal should be most strongly influenced by tissue–iron concentration, particularly in the iron-rich striatum (Haacke et al., 2010; Langkammer et al., 2010). This notion is supported by the searchlight analysis (Fig. 3) that shows the strongest associations with T2* and age occurring in iron-rich areas of the brain (basal ganglia, midbrain) rather than areas with less tissue–iron, e.g. cortex and posterior white matter tracts. Thus developmental differences in striatal neurophysiology as measured with T2* appear to be primarily driven by developmental differences in tissue–iron concentration during adolescence.

It is important to note that although iron is also contained in hemoglobin, the contribution of heme-iron to T2* is negligible compared to that of tissue–iron (Langkammer et al., 2010; Vymazal et al., 1996). The contribution of hemoglobin to magnetic susceptibility only occurs in deoxy-hemoglobin and is greatest at low oxygen saturation (Pauling, 1977), but the paramagnetism of tissue–iron is many times greater than even completely deoxygenated hemoglobin (Vymazal et al., 1996). This small effect of heme-iron is not expected to contribute to the developmental effects observed in this study as its influence on T2* signal should not vary systematically with age in our sample. The vascular system is largely stable during adolescence, with pial vessel coverage and capillary formation (Harris et al., 2011) and total cerebral blood flow volume to the internal carotid artery (the primary blood supply to the striatum) being established by early childhood (Schöning and Hartig, 1996).

4.2. Tissue–iron and the brain

The sensitivity of T2* to tissue–iron is particularly relevant in the context of adolescent development. Iron is transported across the blood–brain barrier via the protein transferrin and stored in cell bodies as ferritin (Aquino et al., 2009; Daugherty and Raz, 2013, Drayer et al., 1986). The basal ganglia and midbrain are the regions of the brain with the greatest ferritin concentration (Haacke et al., 2005; Schenck, 2003). Cells with the greatest ferritin concentration are oligodendrocytes found in both white and gray matter (Haacke et al., 2005). Ferritin can also be found in neurons, particularly those in the basal ganglia (Drayer et al., 1986; Moos, 2002). Within these cells iron contributes to a host of critical neurophysiological processes. In oligodendrocytes, iron is necessary for myelin synthesis and is required for ATP production necessary to sustain the high oxidative metabolism of these cells (Connor and Menzies, 1996; Moos, 2002; Todorich et al., 2009). In the basal ganglia, animal models of iron deficiency (Erikson et al., 2000) and disease models of restless leg syndrome (Connor et al., 2009) and ADHD (Adisetiyo et al., 2014) indicate that tissue–iron is highly related to the dopamine system (Beard and Connor, 2003). In particular, striatal tissue–iron supports D2 receptor expression (Beard, 2003; Jellen et al., 2013), dopamine transmitter function (Adisetiyo et al., 2014; Erikson et al., 2000; Wiesinger et al., 2007), and dopamine neuron excitability (Jellen et al., 2013). As the striatal dopamine system has been shown to develop during adolescence in animal models (Kalsbeek et al., 1988; Rosenberg and Lewis, 1995; Teicher et al., 1995) and has been hypothesized to underlie characteristic behavior and brain function in the adolescent human (Casey et al., 2008; Padmanabhan and Luna, 2014; Spear, 2000), the T2* signal has unique relevance to the study of adolescent striatal development. Furthermore, postmortem (Hallgren and Sourander, 1958) and MRI (Aquino et al., 2009; Wang et al., 2012) studies exploring lifespan differences in tissue–iron have shown general increases in iron concentration in the striatum through middle age and suggest the rate of iron accumulation is greatest in the first two decades of life, indicating a decreased rate of change in accumulation following adolescence.

4.3. T2* and the adolescent brain

The developmental trajectory of T2* signal varied systematically across dorsal and ventral aspects of the striatum. Ventral portions of the striatum, which have predominantly limbic cortical connections (Cohen et al., 2009), showed strong negative relationships with age while dorsal portions, which have predominantly executive and motor cortical connections showed weaker positive relationships with age suggesting that through adolescence and young adulthood limbic and executive striatal systems may have different relative neurophysiological contributions to behavior. Results are in agreement with findings indicating that the striatum has a spatially heterogeneous pattern of development, i.e. the striatal nuclei do not develop in a globally uniform way (Raznahan et al., 2014). The strong negative relationships in ventral striatum indicate consistent increases in tissue–iron concentration with inverse fits suggesting the rate of increase is greatest early in adolescence. Given the association of tissue–iron with both dopamine function and myelination, these increases may support the maturation and proliferation of the dopamine system and myelination of cortico-striatal connections

observed in animal models of adolescent development (e.g. increasing dopamine projections to the primate prefrontal cortex; Rosenberg and Lewis, 1995), supporting the maturation of motivational circuitry.

The developmental trajectory of striatal T2* is unique over adolescence in portions of the caudate and putamen. In these areas, voxel values of T2* varied non-linearly with age, in some cases peaking over adolescence between ages 17 and 18. Of particular interest are positive quadratic relationships ("U" shaped) in the ventral putamen that indicate peak tissue–iron concentration in this region over adolescence, possibly relating peaks in dopamine D2 receptor expression observed in the rodent (Teicher et al., 1995) and hypothesized to occur in the human (Casey et al., 2008). Overall, these nonlinear developmental trajectories suggest a period of striatal neurophysiological maturation that may contribute to observed peaks in sensation seeking and risk-taking behavior and striatal reward sensitivity during this stage of development (Padmanabhan et al., 2011; Spear, 2000), while linear relationships may reflect continued motivational system development through young adulthood (Arnett, 1999; Hoogendam et al., 2013). Given findings in animal models indicating adolescent peaks in dopamine receptor expression and human fMRI studies suggesting peak ventral striatal reactivity under certain incentive contexts, we were surprised to observe linear or inverse associations of T2* with age in portions of striatum. It is possible that increases in adolescent BOLD response to reward may be sensitive to additional aspects of DA function to which tissue–iron is not directly related, such as DA release quantity or probability, which may have different developmental trajectories. The observed pattern of effects likely also reflects the indirect nature of the relationship between tissue–iron and dopamine receptor density and DAT function as well as its role in many other neurophysiological processes (e.g. myelination and ATP production) that do not decrease in adulthood. Speculatively, it may be that individual differences in T2* and basal ganglia tissue–iron concentration relate to individual differences in indices of the structure and function of the dopamine system. Clearly, further research is needed to directly characterize this relationship, particularly in normative populations.

Quantitatively, the voxel-wise distribution of feature weights from the multivariate support vector regression indicate that neurophysiological maturation of the striatum is most strongly influenced by the continued maturation of the ventral striatum, including the nucleus accumbens and ventromedial portions of the caudate and putamen, into adulthood. During adolescence, the ventral striatum exhibits peak functional reactivity to reward stimuli under certain incentive contexts and is associated with risk-taking behavior during this period (Ernst et al., 2005; Galvan et al., 2006, 2007; Geier et al., 2010; Padmanabhan et al., 2011). Furthermore, this region is highly dopamine innervated and is a central component of the frontostriatal dopamine reward pathways (Knutson and Cooper, 2005, McGinty et al., 2013, Puglisi-Allegra and Ventura, 2012) hypothesized to underlie sensation seeking and risk-taking behavior (Blum et al., 2000, Spear, 2000). Speculatively, increases in tissue–iron concentration in this region may thus be mechanistically related to adolescent behavior and striatal reward reactivity through its association with dopamine receptor expression, transporter function, and excitability (Erikson et al., 2000; Jellen et al., 2013; Wiesinger et al., 2007) and myelination (Connor and Menzies, 1996; Moos, 2002; Todorich et al., 2009) within cortico-ventral striatal pathways.

An exploratory whole-brain analysis revealed that the strongest associations between T2* and age occur in ventromedial subcortical and midbrain regions known to be the most dopamine and iron-rich areas of the brain (Drayer et al., 1986; Haacke et al., 2005; Langkammer et al., 2010) with rates of iron accumulation fluctuating across the lifespan (Aquino et al., 2009; Haacke et al., 2010; Hallgren and Sourander, 1958). In the cortex, significant associations were observed in frontal limbic areas that fall along the mesolimbic and mesocortical dopamine pathways as well as frontal executive and motor regions. It should be noted that the interpretation of precise neurophysiological properties underlying of the T2* signal outside of the iron-rich striatum is somewhat less straightforward. For example, the degree to which cortical T2* reflects tissue–iron concentration per se is less clear as myelination should have a larger relative contribution to the signal in areas that contain lower levels of tissue–iron (e.g. cortex, white matter). For this reason, it may be advisable for future researchers to focus T2* analyses to brain areas known to have high concentrations of tissue–iron (e.g. the basal ganglia and midbrain). Nevertheless, this collection of cortical and subcortical brain regions are consistent with our striatal findings in that they are structurally and functionally connected within the dopamine system and have been shown to be sensitive to adolescent development (Casey et al., 2008; Cohen et al., 2009; Galvan et al., 2006; Geier et al., 2010; Giedd et al., 1999; Hwang et al., 2010; Lehéricy et al., 2004; Martino et al., 2008; Sowell et al., 1999). As such, these results provide evidence in support of the hypothesis that neurophysiological development of the frontostriatal dopamine circuit in humans occurs over adolescence (Casey et al., 2008; Spear, 2000).

4.4. Limitations and future directions

Our findings, along with those of Vo et al. (2011), suggest that T2*-weighted EPI data may be a useful tool for the investigation of striatal neurophysiology. An advantage of this method is that this measure can be derived from existing fMRI datasets, whether they be resting-state or task-related. As mentioned above, we recommend focusing future analyses on the basal ganglia and other brain areas known to have relatively high concentrations of tissue–iron as the interpretability of the neurophysiological mechanisms contributing to T2* is greatest in these areas. Additionally, we recommend brain areas such as ventral orbitofrontal cortex and portions of inferotemporal cortex that are prone to susceptibility artifacts be avoided for T2*-weighted EPI analyses. We wish to note that investigators interested in specifically quantifying tissue–iron concentrations could also apply quantitative MR sequences, such as R2′ or R2*, that have been shown to be linearly related to

tissue–iron content (Sedlacik et al., 2014; Yao et al., 2009) to assess this tissue property more precisely. An important direction for future work is to directly characterize the association between tissue–iron concentration in the basal ganglia and indices of dopamine system function in normative populations, expanding on work done in RLS, ADHD, and iron-deficient populations and leading to greater functional interpretability and significance of T2* and related measures. Of course, an enhanced understanding of this relationship has powerful implications for human developmental studies in which more invasive imaging techniques capable of assessing the neurobiology of the dopamine system are not available. Finally, though this study was performed using a large cross-sectional dataset that covered a wide age-range, future work should employ a longitudinal design in order to better asses age-related *changes* in T2*, per se.

5. Conclusion

Our results provide in vivo evidence of continued neurophysiological maturation of striatal regions throughout human adolescence. Our findings and the nature of the T2* signal suggest that age related differences in striatal neurophysiology are most strongly influenced by differences in tissue–iron concentration (Aoki et al., 1989; Chavhan et al., 2009, Daugherty and Raz, 2013; He and Yablonskiy, 2009; Langkammer et al., 2010; Schenck, 2003). Given the contribution of this tissue property to brain function, including dopamine function, and the role of the striatum in learning, motivation, and reward processing, protracted maturation of the striatum as indexed by T2* may strongly contribute to known developmental changes in behavior and brain function through adolescence.

Authors' contributions

B. Larsen and B. Luna collaborated in conceiving and designing the experiment. B. Larsen analyzed the data and wrote the initial draft of the paper. B. Luna provided edits of the original manuscript.

Conflicts of interest

None to report.

Acknowledgments

The project described was supported by grant number 5R01 MH080243 from the National Library of Medicine, National Institutes of Health. The contents of this report are solely the responsibility of the authors and do not necessarily represent the official views of the National Library of Medicine or NIH, DHHS.

Appendix A. Supplementary data

Supplementary data associated with this article can be found, in the online version, at http://dx.doi.org/10.1016/j.dcn.2014.12.003.

References

Adisetiyo, V., Jensen, J.H., Tabesh, A., Deardorff, R.L., Fieremans, E., et al., 2014. Multimodal MR imaging of brain iron in attention deficit hyperactivity disorder: a noninvasive biomarker that responds to psychostimulant treatment? Radiology 272 (2), 524–532.

Alexander, G.E., DeLong, M.R., Strick, P.L., 1986. Parallel organization of functionally segregated circuits linking basal ganglia and cortex. Annu. Rev. Neurosci. 9, 357–381.

Aoki, S., Okada, Y., Nishimura, K., Barkovich, A.J., Kjos, B.O., et al., 1989. Normal deposition of brain iron in childhood and adolescence: MR imaging at 1.5 T. Radiology 172 (2), 381–385.

Aquino, D., Bizzi, A., Grisoli, M., Garavaglia, B., Bruzzone, M.G., et al., 2009. Age-related iron deposition in the basal ganglia: quantitative analysis in healthy subjects? Radiology 252 (1), 165–172.

Arnett, J.J., 1999. Adolescent storm and stress, reconsidered. Am. Psychol. 54 (5), 317–326.

Beard, J., 2003. Iron deficiency alters brain development and functioning? J. Nutr. 133 (5), 1468S–1472S.

Beard, J.L., Connor, J.R., 2003. Iron status and neural functioning. Annu. Rev. Nutr. 23, 41–58.

Beaulieu, J.-M., Gainetdinov, R.R., 2011. The physiology, signaling, and pharmacology of dopamine receptors. Pharmacol. Rev. 63 (1), 182–217.

Bjork, J.M., Knutson, B., Fong, G.W., Caggiano, D.M., Bennett, S.M., Hommer, D.W., 2004. Incentive-elicited brain activation in adolescents: similarities and differences from young adults? J. Neurosci. 24 (8), 1793–1802.

Blum, K., Braverman, E.R., Holder, J.M., Lubar, J.F., Monastra, V.J., et al., 2000. Reward deficiency syndrome: a biogenetic model for the diagnosis and treatment of impulsive, addictive, and compulsive behaviors. J. Psychoact. Drugs 32 (Suppl. i–iv), 1–112.

Bradshaw, J.L., Sheppard, D.M., 2000. The neurodevelopmental frontostriatal disorders: evolutionary adaptiveness and anomalous lateralization? Brain Lang. 73 (2), 297–320.

Burges Christopher, J.C., 1998. A tutorial on support vector machines for pattern recognition. Data Min. Knowl. Discov. 2, 121–167.

Casey, B.J., Jones, R.M., Hare, T.A., 2008. The adolescent brain. Ann. N. Y. Acad. Sci. 1124, 111–126.

Caviness, V.S., Kennedy, D.N., Richelme, C., Rademacher, J., Filipek, P.A., 1996. The human brain age 7–11 years: a volumetric analysis based on magnetic resonance images. Cereb. Cortex 6 (726), 736.

Chambers, R.A., Taylor, J.R., Potenza, M.N., 2003. Developmental neurocircuitry of motivation in adolescence: a critical period of addiction vulnerability? Am. J. Psychiatry 160 (6), 1041–1052.

Chang, C.-C., Lin, C.-J., 2011. LIBSVM: a library for support vector machines. ACM Trans. Intell. Syst. Technol. 2 (3), 1–27.

Chavhan, G.B., Babyn, P.S., Thomas, B., Shroff, M.M., Haacke, E.M., 2009. Principles, techniques, and applications of T2*-based MR imaging and its special applications. Radiographics 29 (5), 1433–1449.

Chih-Wei, H., Chang, C.-C., Lin, C.-J., 2003. A Practical Guide to Support Vector Classification.

Cohen, M.X., Schoene-Bake, J.-C., Elger, C.E., Weber, B., 2009. Connectivity-based segregation of the human striatum predicts personality characteristics? Nat. Neurosci. 12 (1), 32–34.

Connor, J.R., Menzies, S.L., 1996. Relationship of iron to oligodendrocytes and myelination? Glia 17 (2), 83–93.

Connor, J.R., Wang, X.-S., Allen, R.P., Beard, J.L., Wiesinger, J.A., et al., 2009. Altered dopaminergic profile in the putamen and substantia nigra in restless leg syndrome? Brain 132 (9), 2403–2412.

Cox, R.W., 1996. AFNI: software for analysis and visualization of functional magnetic resonance neuroimages? Comput. Biomed. Res. Int. J. 29 (3), 162–173.

Crews, F., He, J., Hodge, C., 2007. Adolescent cortical development: a critical period of vulnerability for addiction? Pharmacol. Biochem. Behav. 86 (2), 189–199.

Crone, E.A., Dahl, R.E., 2012. Understanding adolescence as a period of social-affective engagement and goal flexibility. Nat. Rev. Neurosci. 13, 636–650.

Daugherty, A., Raz, N., 2013. Age-related differences in iron content of subcortical nuclei observed in vivo: a meta-analysis. Neuroimage 70, 113–121.

Dosenbach, N.U.F., Nardos, B., Cohen, A.L., Fair, D.A., Power, J.D., et al., 2010. Prediction of Individual Brain Maturity Using fMRI? Science 329 (5997), 1358–1361.

Drayer, B., Burger, P., Darwin, R., Riederer, S., Herfkens, R., Johnson, G.A., 1986. MRI of brain iron? AJR Am. J. Roentgenol. 147 (1), 103–110.

Eaton, D.K., Kann, L., Kinchen, S., Ross, J., Hawkins, J., et al., 2006. Youth risk behavior surveillance – United States 2005. J. Sch. Health 76 (7), 353–372.
Erikson, K.M., Jones, B.C., Beard, J.L., 2000. Iron deficiency alters dopamine transporter functioning in rat striatum? J. Nutr. 130 (11), 2831–2837.
Ernst, M., Nelson, E.E., Jazbec, S., McClure, E.B., Monk, C.S., et al., 2005. Amygdala and nucleus accumbens in responses to receipt and omission of gains in adults and adolescents? Neuroimage 25 (4), 1279–1291.
Eshel, N., Nelson, E.E., Blair, J., Pine, D.S., Ernst, M., 2007. Neural substrates of choice selection in adults and adolescents: development of the ventrolateral prefrontal and anterior cingulate cortices? Neuropsychologia 45 (6), 1270–1279.
Galvan, A., Hare, T.A., Parra, C.E., Penn, J., Voss, H., et al., 2006. Earlier development of the accumbens relative to orbitofrontal cortex might underlie risk-taking behavior in adolescents? J. Neurosci. Off. J. Soc. Neurosci. 26 (25), 6885–6892.
Galvan, A., Hare, T., Voss, H., Glover, G., Casey, B.J., 2007. Risk-taking and the adolescent brain: who is at risk? Dev Sci. 10 (2), F8–F14.
Geier, C.F., Terwilliger, R., Teslovich, T., Velanova, K., Luna, B., 2010. Immaturities in reward processing and its influence on inhibitory control in adolescence? Cereb. Cortex N. Y. N 1991 20 (7), 1613–1629.
Giedd, J.N., Blumenthal, J., Jeffries, N.O., Castellanos, F.X., Liu, H., et al., 1999. Brain development during childhood and adolescence: a longitudinal MRI study? Nat. Neurosci. 2 (10), 861–863.
Haacke, E.M., Ayaz, M., Khan, A., Manova, E.S., Krishnamurthy, B., et al., 2007. Establishing a baseline phase behavior in magnetic resonance imaging to determine normal vs. abnormal iron content in the brain. J. Magn. Reson. Imaging 26 (2), 256–264.
Haacke, E.M., Cheng, N.Y.C., House, M.J., Liu, Q., Neelavalli, J., et al., 2005. Imaging iron stores in the brain using magnetic resonance imaging? Magn. Reson. Imaging 23 (1), 1–25.
Haacke, E.M., Xu, Y., Cheng, Y.-C.N., Reichenbach, J.R., 2004. Susceptibility weighted imaging (SWI). Magn. Reson. Med. 52 (3), 612–618.
Haacke, E.M., Miao, Y., Liu, M., Habib, C.A., Katkuri, Y., et al., 2010. Correlation of change in R2* and phase with putative iron content in deep gray matter of healthy adults? J. Magn. Reson. Imaging 32 (3), 561–576.
Haber, S.N., Knutson, B., 2010. The reward circuit: linking primate anatomy and human imaging? Neuropsychopharmacology 35 (1), 4–26.
Hallgren, B., Sourander, P., 1958. The effect of age on the non-haemin iron in the human brain? J. Neurochem. 3 (1), 41–51.
Harris, J.J., Reynell, C., Attwell, D., 2011. The physiology of developmental changes in BOLD functional imaging signals? Dev. Cogn. Neurosci. 1 (3), 199–216.
He, X., Yablonskiy, D.A., 2009. Biophysical mechanisms of phase contrast in gradient echo MRI? Proc. Natl. Acad. Sci. U. S. A. 106 (32), 13558–13563.
Hoogendam, J.M., Kahn, R.S., Hillegers, M.H.J., van Buuren, M., Vink, M., 2013. Different developmental trajectories for anticipation and receipt of reward during adolescence. Dev. Cogn. Neurosci. 6, 113–124.
Hwang, K., Hallquist, M.N., Luna, B., 2013. The development of hub architecture in the human functional brain network? Cereb. Cortex N. Y. N 1991 23 (10), 2380–2393.
Hwang, K., Velanova, K., Luna, B., 2010. Strengthening of top-down frontal cognitive control networks underlying the development of inhibitory control: an fMRI effective connectivity study? J. Neurosci. 30 (46), 15535–15545.
Jellen, L.C., Lu, L., Wang, X., Unger, E.L., Earley, C.J., et al., 2013. Iron deficiency alters expression of dopamine-related genes in the ventral midbrain in mice. Neuroscience 252, 13–23.
Kalsbeek, A., Voorn, P., Buijs, R.M., Pool, C.W., Uylings, H.B., 1988. Development of the dopaminergic innervation in the prefrontal cortex of the rat? J. Comp. Neurol. 269 (1), 58–72.
Knutson, B., Cooper, J.C., 2005. Functional magnetic resonance imaging of reward prediction? Curr. Opin. Neurol. 18 (4), 411–417.
Kriegeskorte, N., Goebel, R., Bandettini, P., 2006. Information-based functional brain mapping? Proc. Natl. Acad. Sci. U. S. A. 103 (10), 3863–3868.
Langkammer, C., Krebs, N., Goessler, W., Scheurer, E., Ebner, F., et al., 2010. Quantitative MR imaging of brain iron: a postmortem validation study? Radiology 257 (2), 455–462.
Langkammer, C., Krebs, N., Goessler, W., Scheurer, E., Yen, K., et al., 2012. Susceptibility induced gray-white matter MRI contrast in the human brain? Neuroimage 59 (2–5), 1413–1419.
Lehéricy, S., Ducros, M., Van de Moortele, P.-F., Francois, C., Thivard, L., et al., 2004. Diffusion tensor fiber tracking shows distinct corticostriatal circuits in humans? Ann. Neurol. 55 (4), 522–529.
Leijenhorst, L.V., Zanolie, K., Meel, C.S.V., Westenberg, P.M., Rombouts, S.A.R.B., Crone, E.A., 2010. What motivates the adolescent? Brain regions mediating reward sensitivity across adolescence. Cereb. Cortex 20 (1), 61–69.
Luna, B., Garver, K.E., Urban, T.A., Lazar, N.A., Sweeney, J.A., 2004. Maturation of cognitive processes from late childhood to adulthood. Child Dev. 75, 1357–1372.
Luts, J., Ojeda, F., Van de Plas, R., De Moor, B., Van Huffel, S., Suykens, J.A.K., 2010. A tutorial on support vector machine-based methods for classification problems in chemometrics? Anal. Chim. Acta 665 (2), 129–145.
Martinez, D., Slifstein, M., Broft, A., Mawlawi, O., Hwang, D.-R., et al., 2003. Imaging human mesolimbic dopamine transmission with positron emission tomography, Part II: amphetamine-induced dopamine release in the functional subdivisions of the striatum. J. Cereb. Blood Flow Metab. Off. J. Int. Soc. Cereb. Blood Flow Metab. 23 (3), 285–300.
Martino, A.D., Scheres, A., Margulies, D.S., Kelly, A.M.C., Uddin, L.Q., et al., 2008. Functional connectivity of human striatum: a resting state fMRI study? Cereb. Cortex 18 (12), 2735–2747.
McClure, S.M., Berns, G.S., Montague, P.R., 2003. Temporal prediction errors in a passive learning task activate human striatum? Neuron 38 (2), 339–346.
McGinty, V.B., Lardeux, S., Taha, S.A., Kim, J.J., Nicola, S.M., 2013. Invigoration of reward seeking by cue and proximity encoding in the nucleus accumbens? Neuron 78 (5), 910–922.
Middleton, F.A., Strick, P.L., 2000. Basal ganglia and cerebellar loops: motor and cognitive circuits. Brain Res. Rev. 31 (2–3), 236–250.
Misaki, M., Kim, Y., Bandettini, P.A., Kriegeskorte, N., 2010. Comparison of multivariate classifiers and response normalizations for pattern-information fMRI? Neuroimage 53 (1), 103–118.
Misaki, M., Luh, W.-M., Bandettini, P.A., 2013. The effect of spatial smoothing on fMRI decoding of columnar-level organization with linear support vector machine? J. Neurosci. Methods 212 (2), 355–361.
Moos, T., 2002. Brain iron homeostasis? Dan. Med. Bull. 49 (4), 279–301.
Padmanabhan, A., Geier, C.F., Ordaz, S.J., Teslovich, T., Luna, B., 2011. Developmental changes in brain function underlying the influence of reward processing on inhibitory control? Dev. Cogn. Neurosci. 1 (4), 517–529.
Padmanabhan, A., Luna, B., 2014. Developmental imaging genetics: linking dopamine function to adolescent behavior. Brain Cogn. 89, 27–38.
Pauling, L., 1977. Magnetic properties and structure of oxyhemoglobin? Proc. Natl. Acad. Sci. U. S. A. 74 (7), 2612–2613.
Paulsen, D.J., Hallquist, M.N., Geier, C.F., Luna, B., 2014. Effects of incentives, age, and behavior on brain activation during inhibitory control: A longitudinal fMRI study. Dev. Cogn. Neurosci., http://dx.doi.org/10.1016/j.dcn.2014.09.003, e-pub ahead of print.
Pereira, F., Mitchell, T., Botvinick, M., 2009. Machine learning classifiers and fMRI: a tutorial overview. Neuroimage 45 (1 Suppl.), S199–S209.
Postuma, R.B., Dagher, A., 2006. Basal ganglia functional connectivity based on a meta-analysis of 126 positron emission tomography and functional magnetic resonance imaging publications? Cereb. Cortex 16 (10), 1508–1521.
Puglisi-Allegra, S., Ventura, R., 2012. Prefrontal/accumbal catecholamine system processes emotionally driven attribution of motivational salience. Rev. Neurosci. 23 (5–6).
Raznahan, A., Shaw, P.W., Lerch, J.P., Clasen, L.S., Greenstein, D., et al., 2014. Longitudinal four-dimensional mapping of subcortical anatomy in human development? Proc. Natl. Acad. Sci. 111 (4), 1592–1597.
Rosenberg, D.R., Lewis, D.A., 1995. Postnatal maturation of the dopaminergic innervation of monkey prefrontal and motor cortices: a tyrosine hydroxylase immunohistochemical analysis? J. Comp. Neurol. 358 (3), 383–400.
Schenck, J.F., 2003. Magnetic resonance imaging of brain iron. J. Neurol. Sci. 207 (1–2), 99–102.
Schöning, M., Hartig, B., 1996. Age dependence of total cerebral blood flow volume from childhood to adulthood? J. Cereb. Blood Flow Metab. 16 (5), 827–833.
Sedlacik, J., Boelmans, K., Löbel, U., Holst, B., Siemonsen, S., Fiehler, J., 2014. Reversible, irreversible and effective transverse relaxation rates in normal aging brain at 3 T. Neuroimage 84, 1032–1041.
Smith, S.M., Jenkinson, M., Woolrich, M.W., Beckmann, C.F., Behrens, T.E.J., et al., 2004. Advances in functional and structural MR image analysis and implementation as FSL. Neuroimage 23 (Suppl. 1), S208–S219.
Sowell, E.R., Thompson, P.M., Holmes, C.J., Jernigan, T.L., Toga, A.W., 1999. In vivo evidence for post-adolescent brain maturation in frontal and striatal regions? Nat. Neurosci. 2 (10), 859–861.
Spear, L.P., 2000. The adolescent brain and age-related behavioral manifestations? Neurosci. Biobehav. Rev. 24 (4), 417–463.

Tarazi, F.I., Tomasini, E.C., Baldessarini, R.J., 1998. Postnatal development of dopamine and serotonin transporters in rat caudate-putamen and nucleus accumbens septi? Neurosci. Lett. 254 (1), 21–24.

Teicher, M.H., Andersen, S.L., Hostetter Jr., J.C., 1995. Evidence for dopamine receptor pruning between adolescence and adulthood in striatum but not nucleus accumbens. Brain Res. Dev. Brain Res. 89 (2), 167–172.

Todorich, B., Pasquini, J.M., Garcia, C.I., Paez, P.M., Connor, J.R., 2009. Oligodendrocytes and myelination: the role of iron? Glia 57 (5), 467–478.

Vapnik, V.N., 1999. An overview of statistical learning theory. IEEE Trans. Neural Netw. 10 (5), 988–999.

Vo, L.T.K., Walther, D.B., Kramer, A.F., Erickson, K.I., Boot, W.R., et al., 2011. Predicting individuals' learning success from patterns of pre-learning MRI activity. PLoS ONE 6 (1), e16093.

Vymazal, J., Brooks, R.A., Baumgarner, C., Tran, V., Katz, D., et al., 1996. The relation between brain iron and NMR relaxation times: an in vitro study. Magn. Reson. Med. 35 (1), 56–61.

Wang, J., Shaffer, M.L., Eslinger, P.J., Sun, X., Weitekamp, C.W., et al., 2012. Maturational and aging effects on human brain apparent transverse relaxation. PLoS ONE 7 (2), e31907.

Wiesinger, J.A., Buwen, J.P., Cifelli, C.J., Unger, E.L., Jones, B.C., Beard, J.L., 2007. Down-regulation of dopamine transporter by iron chelation in vitro is mediated by altered trafficking, not synthesis. J. Neurochem. 100 (1), 167–179.

Yao, B., Li, T.-Q., van Gelderen, P., Shmueli, K., de Zwart, J.A., Duyn, J.H., 2009. Susceptibility contrast in high field MRI of human brain as a function of tissue iron content? Neuroimage 44 (4), 1259–1266.